Climatic variations during the Holocene inferred from radiocarbon and stable carbon isotopes in a high-alpine cave

Caroline Welte[1,2], Jens Fohlmeister[3,4], Melina Wertnik[1,2], Lukas Wacker[1], Bodo Hattendorf[5], Timothy I. Eglinton[2], Christoph Spötl[6]

[1] Laboratory of Ion Beam Physics, ETHZ, Otto-Stern Weg 5, 8093 Zurich, Switzerland,

[2] Geological Institute, ETHZ, Sonnegstrasse 5, 8092 Zurich, Switzerland

[3] Potsdam Institute for Climate Impact Research, Telegrafenberg, 14473 Potsdam, Germany

[4] GFZ German Research Centre for Geosciences, Section 'Climate Dynamics and Landscape Development', 14473 Potsdam, Germany

[5] Laboratory of Inorganic Chemistry, D-CHAB, ETHZ, Vladimir-Prelog Weg 1, 8093 Zurich, Switzerland

[6] Institute of Geology, University of Innsbruck, Innrain 52f, 6020 Innsbruck, Austria

Correspondence to: Caroline Welte: cwelte@phys.ethz.ch, Jens Fohlmeister: jens.fohlmeister@pik-potsdam.de

Abstract

Rapid and continuous analysis of radiocarbon (^{14}C) concentration in carbonate samples at very high spatial resolution has been made possible with the new LA-AMS (laser ablation accelerator mass spectrometry) technique. This novel approach can provide radiocarbon data at a spatial resolution similar to that of stable carbon (C) isotope measurements by isotope ratio mass spectrometry (IRMS) and, thus, can help to interpret δ^{13}C signatures, which otherwise are difficult to understand due to numerous processes contributing to changes in C-isotope ratio. In this work, we analyzed δ^{13}C and ^{14}C on the Holocene stalagmite SPA 127 from the high-alpine Spannagel Cave (Austria). Both proxies respond in a complex manner to climate variability. Combined stable carbon and radiocarbon profiles allow to identify three growth periods characterized by different δ^{13}C signatures: (i) the period 8.5 to 8.0 ka BP is characterized by relatively low δ^{13}C values with small variability combined with a comparably high radiocarbon reservoir effect (expressed as dead carbon fraction, dcf) of around 60%. This points towards C contributions of host rock dissolution and/or from an "old" organic matter (OM) reservoir in the karst potentially mobilized due to the warm climatic conditions of the early Holocene. (ii) Between 8 and 3.8 ka BP a strong variability in δ^{13}C reaching values from -8 to +1‰ with a generally lower dcf was observed. The δ^{13}C variability is most likely caused by changes in gas exchange processes in the cave, which are induced by reduced drip rates as derived from reduced stalagmite growth rates. Additionally, the lower dcf indicates that the OM reservoir contributed less to stalagmite growth in this period possibly as a result of reduced meteoric precipitation or because it was exhausted. (iii) In the youngest section between 3.8 and 2.4 ka BP, comparably stable and low δ^{13}C values combined with an increasing dcf reaching up to 50% again hint towards a contribution of an aged OM reservoir in the karst. This study reveals the high potential of combining high-resolution ^{14}C profiles in speleothems with δ^{13}C records in order to disentangle climate-related C dynamics in karst systems.

1 Introduction

Understanding the climate of the past is the key for understanding how climate and environment will change in the future. Insights into paleoclimate are gained through the study of archives with stalagmites being a prominent example for a terrestrial archive. Stalagmites can grow continuously over thousands to tens of thousands of years (Cheng et al., 2016; Fairchild et al., 2006; Moseley et al., 2020). Caves hosting stalagmites are present on all continents except Antarctica and uranium-series disequilibrium dating allows to build robust chronologies (Richards and Dorale, 2003; Scholz and Hoffmann, 2008). Trace-element and stable isotope data of stalagmites allow the reconstruction of climatic conditions in the past. For example, the oxygen isotope composition (δ^{18}O) is generally interpreted as a combination of a temperature and a meteoric precipitation signal (Lachniet, 2009; Wackerbarth et al., 2010). The interpretation of the stable carbon isotope signature (δ^{13}C), however, is more challenging since additional local effects, such as vegetation changes (e.g., Bar-Matthews et al., 1999; Denniston et al., 2007; Fohlmeister et al., 2020), the carbonate dissolution mechanism (e.g., Fohlmeister et al., 2010b; Lechleitner et al., 2016), and in-cave fractionation processes (e.g., Mattey et al., 2016; Spötl et al., 2005) may have an influence and little is known about the relative magnitude of these processes. Besides the stable C isotopes, radiocarbon (^{14}C) decaying with a half-life of ~5700 yrs (Kutschera, 2013) can be a valuable tool in speleothem research (e.g., Bajo et al., 2017; Lechleitner et al., 2016). So far, this isotope has not been fully exploited in speleothem science, mostly due to the time-consuming sampling and processing as well as the comparably high costs associated with these analyses. However, recently both issues have been considerably improved by invention

2

(Welte et al., 2016a; Welte et al., 2016b) and advances in laser ablation coupled to accelerator mass spectrometry (LA-AMS; Welte et al., 2017; Yeman et al., 2020), which can be well applied to carbonate material.

We investigated a stalagmite that grew in the Spannagel cave system (Tyrol, Austria; Spötl et al., 2004) by means of C isotope systematics. This high-alpine cave system was investigated in many studies in the context of palaeoclimate and palaeoenvironmental research mostly using O isotopes and growth phases as proxies (e.g.,Fohlmeister et al., 2013; Spötl and Mangini, 2010). The gneiss covering the cave-bearing marble contains interspersed fine-crystalline pyrite and is topped by a thin soil layer with sparse vegetation. It was hypothesized that the oxidation of pyrite contributes considerably to the dissolution of the host-rock marble and, hence, to the growth of stalagmites and flowstones, in particular during cold climate periods when there is no soil present at this high altitude (Spötl and Mangini, 2007). During some interglacials including the Holocene, when Alpine soils are present in the catchment of the cave´s drip water, sulfide oxidation and soil-derived CO_2 may operate in tandem. Consequently, the stable C isotope signal of stalagmites from this cave is expected to be complex.

The aim of this study is to gain deeper insights into the climatically driven C dynamics in this cave by high spatially resolved ^{14}C analyses of a Holocene stalagmite. This study takes advantage of the recently introduced method of LA-AMS (Welte et al., 2016a; Welte et al., 2016b), which reaches a similar spatial resolution as micro-milling for stable isotope analysis (e.g., Spötl and Mattey, 2006). Using the combined ^{14}C and $\delta^{13}C$ records measured in this study as well as the previously published $\delta^{18}O$ signal (Fohlmeister et al., 2013), we explore the key processes influencing the carbon isotope composition of speleothems in this cave and gain a better understanding of the potential and limits of ^{14}C analysis of carbonates using LA-AMS.

2 Radiocarbon and dead carbon fraction

In most karst systems, dissolution of the carbonate host rock is driven by soil-derived carbonic acid. In this case, the two major soil-derived C sources contributing to the $\delta^{13}C$ values of the speleothem are pedogenic CO_2 from the degradation of soil organic matter (SOM) and root respiration that acidifies the meteoric water as it percolates through the soil. Recently, evidence was found for a potential additional C source stemming from CO_2 derived from the oxidation of "old" organic matter (OM) in the deep vadose zone (Bergel et al., 2017; Noronha et al., 2015). The water charged with carbonic acid then dissolves the host rock $CaCO_3$. All of those C-pools have different characteristics with respect to their stable and radiocarbon isotope signatures (Fig. 1).
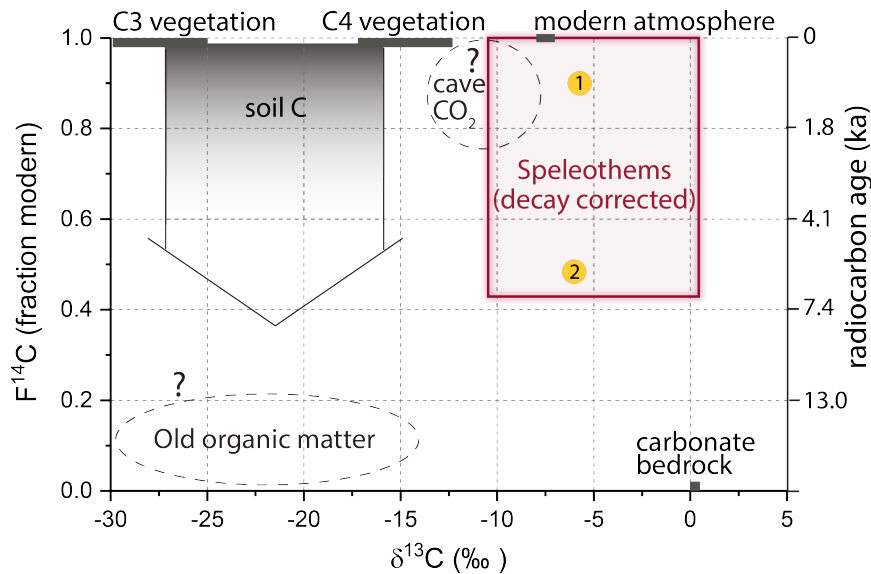
Figure 1: Carbon isotopic signatures of carbon-bearing reservoirs in karst systems. Yellow circles mark speleothem-C resulting from different processes: 1. $CaCO_3$ dissolution via soil CO_2-derived carbonic acid. 2. Deep OC contribution to seepage water feeding speleothems (adapted from Fairchild and Baker (2012)).

When working with radiocarbon in speleothems it is important to determine the reservoir effect (Genty and Massault, 1997). If a radiocarbon-independent chronology for the stalagmite exists, the reservoir effect, which is often termed dead carbon fraction (dcf), can be derived through comparison of the measured ^{14}C profile in the stalagmite ($F^{14}C_{stal}$) with the ^{14}C atmosphere's signature ($F^{14}C_{atm}$) of the same time (Genty and Massault (1997)):

$$dcf = \left(1 - \frac{F^{14}C_{stal}}{F^{14}C_{atm}}\right) \cdot 100\% \qquad (1)$$

Values for dcf range from a few % up to 70% (Bajo et al., 2017; Southon et al., 2012) and commonly vary within a single speleothem with time (Bajo et al., 2017; Noronha et al., 2014; Therre et al., 2020). The magnitude of the dcf is influenced by multiple factors, such as the age of soil OM, contributing to soil gas CO_2 production (Fohlmeister et al., 2011b) and consequently altering the ^{14}C concentration in the stalagmite. Also the CO_2 partial pressure (pCO_2) in the soil plays an important role, with a complex relationship between the amount of soil gas pCO_2 and the dcf (Fohlmeister et al., 2011b). Additionally, the conditions of karst dissolution, i.e. open vs. closed system (Fohlmeister et al., 2011a; Hendy, 1971), affect the dcf. In a more open system, the dcf is low because the percolating water can continuously exchange C isotopes with the soil gas CO_2 leading to a ^{14}C concentration in the stalagmite that is dominated by the near-atmospheric soil ^{14}C signature (Southon et al., 2012). In a more closed system, this exchange is inhibited with the extreme case being a completely closed system, where for each mole of carbonic acid one mole of $CaCO_3$ is dissolved resulting in a dcf of up to 50%. Fractionation and gas exchange processes in the cave are also potential candidates for modulation of the dcf. These main factors driving the dcf in turn are influenced by numerous parameters such as hydrological and environmental conditions above the cave. Several studies (e.g., Bajo et al., 2017; Fohlmeister et al., 2010a; Griffiths et al., 2012; Lechleitner et al., 2016; Noronha et al., 2014) showed that during periods of increased rainfall the dcf in the stalagmite is enhanced. A likely explanation is a shift towards more closed-system conditions (Table 1) under higher meteoric precipitation regimes. It was argued, that under more humid (arid) conditions the pore spaces in soils are clogged with (devoid of) water, leaving less (more) opportunity for C-exchange processes between dissolved inorganic C species and soil gas CO_2 (Fohlmeister et al., 2010).

An increasing number of cave systems have been reported where carbonate dissolution occurs even if no significant soil exists above the cave, indicating climatic conditions less suited for the existence of vegetation cover. Acidic conditions in the seepage water are achieved via oxidation of pyrite or other sulfide minerals disseminated in the bedrock (Bajo et al., 2017; Lauritzen, 2001; Spötl et al., 2016). In this case the C isotope composition in the drip water is dominated by the bedrock, and the dcf is therefore expected to be relatively high (>50%). Under those conditions the $\delta^{13}C$ values of the speleothems reflect those of the (marine-derived) bedrock, i.e. are shifted closer to 0‰ compared to lower $\delta^{13}C$ values of speleothem $CaCO_3$ of around -12 to -10‰ for cave systems with a soil and vegetation cover. An overview of relevant processes as well as the resulting dcf and $\delta^{13}C$ are summarized in Table 1.

Table 1 Simplified summary of expected $\delta^{13}C$ (assuming C3 vegetation cover) and dcf values in stalagmite $CaCO_3$ for different dominant processes. In many karst systems various combinations of these processes complicate the interpretation.

Process		Expected $\delta^{13}C$ (‰)	Expected dcf (%)
Carbonate dissolution via carbonic acid	open-system	< -10‰	Comparably low, i.e. around 10%
	closed-system	> -10‰	Comparably high, i.e. close to 50%
Carbonate dissolution via oxidation of pyrite		Close to 0‰	Very high, i.e. > 50%
"Old" OM contribution to seepage water acidification		< -10‰	Shift towards higher values (> 50% possible)

3 Materials & Methods

3.1 Sample

Spannagel cave is located in the Tux Valley (47.08028°N, 11.67167°E; Zillertal Alps, western Austria) and opens at 2531 m above sea level. It forms a more than 12 km-long system of galleries and short shafts, which developed in a Jurassic marble tectonically overlain by gneiss. This superposition does not only allow for high-precision U-series dating of stalagmites due to their relatively high U contents, but also gives rise to carbonate dissolution via sulfuric acid stemming from pyrite oxidation. The thin alpine soil provides an additional pedogenic source of acidity and the interplay between the two processes is reflected by highly variable stable C isotope values as well as dcf in Spannagel speleothems. Stalagmite SPA 127 was found in the eastern part of the cave system, which was never ice-covered during the Holocene (Fohlmeister et al., 2013). The stalagmite grew from 8.45 to 2.24 ka BP with an average growth rate of approximately 25 μm/a as confirmed by nine U/Th-ages (Fohlmeister et al., 2013). There is no macro- and microscopic evidence for the existence of hiatuses in this specimen. Further evidence for the absence of hiatuses is provided by two additional speleothems, SPA 12 and SPA 128, from the same cave are partly coeval with SPA 127. These additional speleothems have a higher dating density in parts, where SPA 127 has only a few radiometric U-Th dating points and also do not show evidence of hiatuses (Fohlmeister et al., 2013). In combination with the well replicated stable O isotope signals we are confident that the growth of SPA 127 was not affected by hiatuses.

The 15 cm-long polished slab of the stalagmite analyzed in this study was first used for stable oxygen and carbon isotope analysis where sampling was performed along the extension axis. For LA-AMS analysis, the same section

142 was used but broken in two pieces at a distance from top (dft) of approximately 10 cm, which will be referred to
143 as "top piece" and "bottom piece".

144   1.   Stable isotope analysis

145 Subsamples for stable carbon isotope analysis were micromilled at 100 μm increments and measured using an
146 automated online carbonate preparation system linked to a triple collector gas source mass spectrometer
147 (Delta^{plus}XL, ThermoFisher, Bremen, Germany) at the University of Innsbruck. Values are reported relative to the
148 Vienna Pee Dee Belemnite standard. The long-term precision of the $\delta^{13}C$ values (1 standard deviation of replicate
149 analyses) is 0.06% (Spötl, 2011). The respective $\delta^{18}O$ values have been published earlier (Fohlmeister et al., 2013).

150

3.2 Radiocarbon analysis using LA-AMS

152 By focusing a laser on the surface of a solid sample at sufficiently high energy densities, a small portion of material
153 is ablated and can be used for trace element or isotopic analysis allowing for fast and spatially resolved analysis
154 (Gray, 1985; Koch and Guenther, 2011). ^{14}C analysis of SPA 127 was performed by LA coupled with AMS (Welte
155 et al., 2016a; Welte et al., 2017). For this study, a slightly modified LA-AMS setup was used reaching a smaller
156 spot size (75x140 μm^2) and higher energy densities of up to 8 J/cm^2 allowing for increased signal intensities, i.e.
157 ^{12}C-currents. With LA-AMS a quasi-continuous data stream is produced at 10 sec intervals in the AMS. This is
158 the minimal integration time of the AMS and together with the laser spot width d and the scanning velocity v
159 defines the spatial resolution R according to R = d + v · 10 sec.

160 LA-scans were placed as close as possible to the stable isotope tracks in order to facilitate matching between the
161 two data sets (Fig. 2). However, the LA-AMS setup does not permit to place laser tracks close to the rim of samples
162 causing an offset between the two sampling lanes of approximately 5 mm. Speleothem growth layers are often
163 curved, resulting in a potential offset between stable isotope and radiocarbon data of up to several hundred
164 micrometers, with the outer LA-scan appearing somewhat older than the stable isotope record. Since the curvature
165 of the growth layers is most likely variable, a constant correction factor has not been applied.

166 On the "top piece" of SPA 127 two subsequent scans in opposite direction were performed, first from young to
167 old (T1) and then vice versa (T2) on the same track with a scanning velocity of 20 μm/s and a laser energy density
168 of approximately 5 J/cm^2. On the "bottom piece" a total of three analyses were performed: the initial scan from
169 old to young (B1: 10 μm/s, 1-2 J/cm^2) was followed by a second repeated scan from bottom to top (B2: old to
170 young, 25 μm/s, 8 J/cm^2) after removing the top ~0.5 mm of the sample surface by mechanical polishing. The
171 second scan was necessary to ensure that the unusual ^{14}C signature observed in the oldest part of the stalagmite
172 during the first scan (see section "Results") was not the result of a potentially contaminated surface. A final third
173 analysis (B3) consisting of two scans performed in opposite directions was performed at 20 μm/s and 5 J/cm^2.
174 Processing of the raw ^{14}C data was performed using in-house standards also analyzed by LA-AMS for blank
175 subtraction and standard normalization (marble, F^{14}C = 0 and coral standard, F^{14}C = 0.9445 ± 0.0018). A Savitzky-
176 Golay (SG) filter is applied to the recorded ^{14}C signal of B3, which is a smoothing method that reduces noise while
177 maintaining the shape and height of peaks (Savitzky and Golay, 1964). In brief, a polynomial is fitted to a sub-set
178 of the data points and evaluated at the center of the approximation interval. Two parameters, namely the number
179 of points defining the approximation interval and the maximum polynomial order, can be defined. The smoothing
180 has been applied to the two sub-scans of B3 (from "old to young" and vice versa) as well as to the combined data
181 to ensure robustness of the filter. Corresponding uncertainties are estimated from the square root of the sum of the
182 squared difference between the measured F^{14}C value and the SG fit at each point within the interval. This value is

183 then divided by the square root of the difference between the interval length (number of data points) and the
184 maximum order allowed for the polynomial, which is equivalent to the degree of freedom.
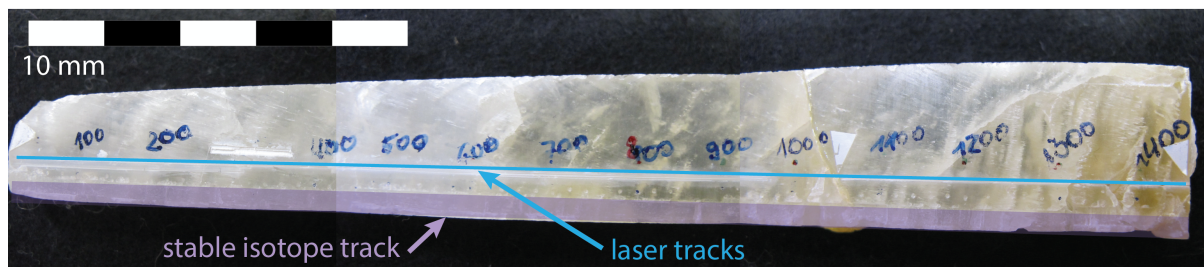
Figure 2: Polished slab of SPA 127 (top is left). Top and bottom piece with location of the stable isotope track marked in purple and LA-AMS test track in blue (the tracks corresponding to the data presented in this work were placed next to the test tracks). The total length of the slab is 14.6 cm.

4 Results

4.1 Dead carbon fraction
[14]C results for both pieces of SPA 127 (T1, T2 and B3) are reported as dcf (blue line in Fig. 3 a and Fig. S8 a). From the ^{14}C profile, the StalAge (Scholz and Hoffmann, 2011) age-depth model was applied to previously published U-Th data (Fohlmeister et al., 2013) and the known ^{14}C content of the atmosphere during the Holocene (Reimer et al., 2013), and the dcf was calculated according to equation (1) for the 1402 radiocarbon data points (Fig. 3 A). A SG filter was applied (interval: 21, maximum polynomial order: 2) and for comparison the $\delta^{18}O$ and $\delta^{13}C$ data are shown in the same graph (Fig. 3 a and b). The U-Th-dates and the corresponding average growth rate calculated using StalAge are displayed in Fig. 4 c.

4.2 Stable C isotopes
The previously published $\delta^{18}O$ values (Fohlmeister et al., 2013) and unpublished $\delta^{13}C$ data (this study) are shown in Fig. 3 a and b, respectively. A large amplitude and fast changes ranging from -8‰ to +1‰ characterize $\delta^{13}C$ throughout the entire length of the speleothem but are especially pronounced between 30 and 130 mm. Layers exhibiting a comparably stable $\delta^{13}C$ occur at the top and bottom of SPA 127, specifically ranging from 0 to 25 mm and from 125 to 150 mm.

5 Discussion
The interpretation of the results on C isotopes in SPA 127 will be divided in three main parts that correspond to three sections identified on the speleothem based on their $\delta^{13}C$ characteristics.

5.1 Old section of SPA 127 (8.5-8.0 ka BP)
In the oldest part of SPA 127, the dcf is comparably high (~60%), while $\delta^{13}C$ is relatively depleted with values lower than -5‰ on average. Although the reservoir effect is extremely high, in principle the obtained C-isotope composition can be explained without a major contribution of pyrite oxidation. The relatively low $\delta^{13}C$ value actually contradicts this mode of host rock dissolution but is in line with a sparse C3 vegetation ($\delta^{13}C \approx$ -25‰) above the cave and host rock dissolution under nearly closed conditions (compare Fig. 4 C and D). The stoichiometry of $CaCO_3$ dissolution by carbonic acid predicts that only about half of the C in the solution is derived from the host rock under nearly completely closed conditions. Given that the Jurassic host rock is devoid of ^{14}C, the biogenic component must be older than the contemporaneous atmosphere to allow dcf values larger than 50%. Thus, in addition to living vegetation, which contributes atmospheric radiocarbon, an "old" OM source, which respires radiocarbon-depleted CO_2, is required to explain depleted $\delta^{13}C$ values and elevated dcf. Such "old" OM

7

218 is also argued to have contributed to the radiocarbon reservoir effect of Moomi Cave (Socotra Island) during the
219 last glacial period (Therre et al., 2020). Observations from other cave and karst systems also point to important C
220 pools deep in the vadose karst, e.g., (Benavente et al., 2010; Bergel et al., 2017; Breecker et al., 2012).
221 Nevertheless, in a sparsely vegetated high elevation region this is the first finding of this kind.

222 The speleothem growth phase prior to 8.0 ka falls coincides with the early Holocene thermal maximum, which is
223 also reflected by the depleted $\delta^{18}O$ values hinting towards higher temperatures (Fohlmeister et al., 2013; Mangini
224 et al., 2005). Warmer periods likely favor microbial decomposition of, e.g., OM present in the epikarst below the
225 soil zone, which leads to an increase in pCO_2 and, hence, more acidic water. In turn, more $CaCO_3$ can be dissolved
226 giving rise to higher speleothem growth rates, which is indeed observed in this period (Fig. 3, orange shaded area).
227 Thus, growth rate and the C-isotope composition of stalagmite SPA 127 are in agreement with the presence of a
228 deep OM reservoir in the karst system above the cave.
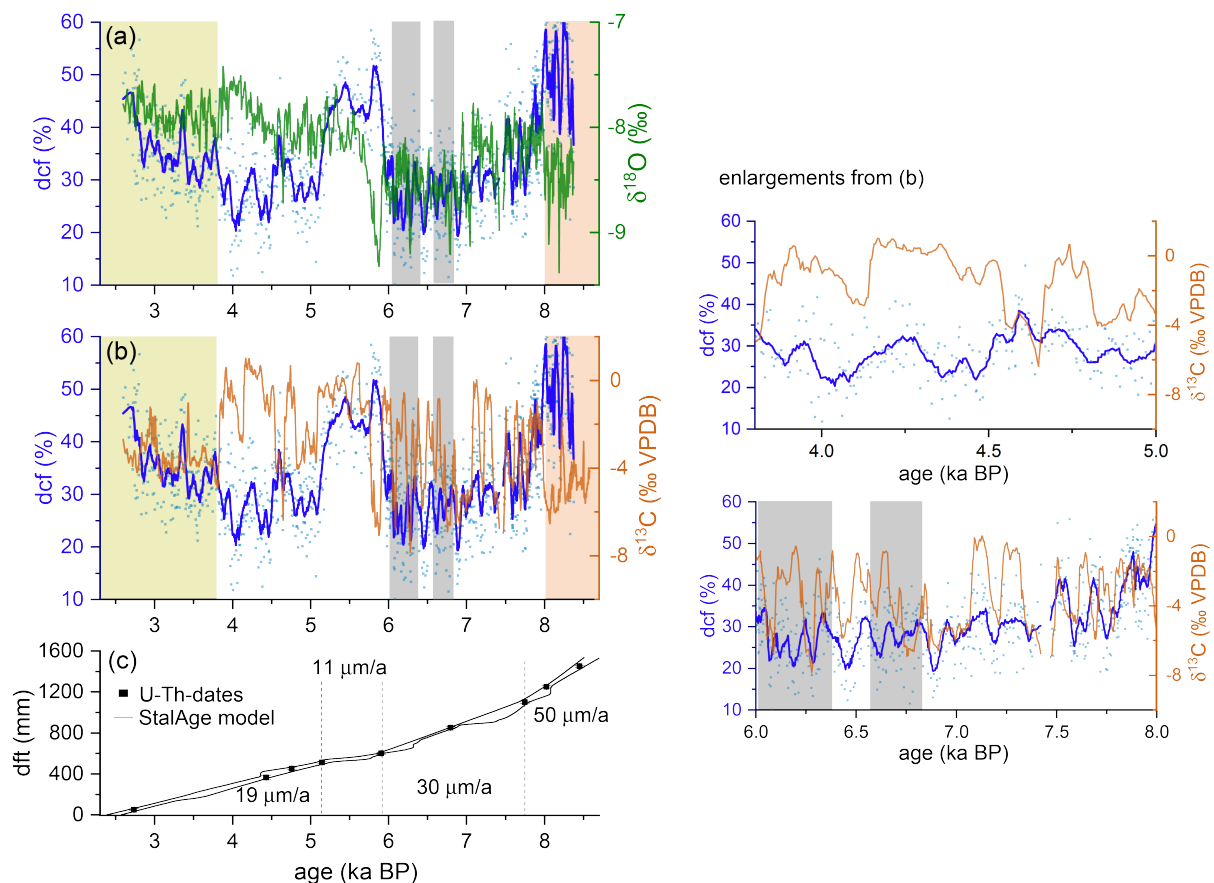
229
230 *Figure 3: Dcf (light blue dots) with a 21 point SG filter (dark blue line) plotted against age and compared to (A) $\delta^{18}O$ (green*
231 *line) (Fohlmeister et al., 2013) and (B) $\delta^{13}C$ (orange line). The yellow, white and orange shaded areas represent phases with*
232 *distinct stable isotope characteristics. Details can be found in the text. Light grey shaded areas mark regions where the SG*
233 *filter was determined with lower confidence. Enlargements of this graph are shown in the right panel. (C) Growth history of*
234 *SPA 127 obtained by StalAge applied to dated depths (black squares, errors are smaller than the symbol size). Numbers*
235 *represent average growth rates ofs the individual sections.*

8

5.2 Rapid changes in dcf and stable C isotopes (8.0 to 3.8 ka BP)

The growth rate was reduced in this period compared to the previous one (Fig. 3). This either suggests that meteoric precipitation or the amount of soil-derived C were reduced, both resulting in a smaller amount of dissolved carbonate transported to the cave. The low $\delta^{13}C$ values of the first growth period were superseded by rapid and very large variations of $\delta^{13}C$. This pattern is complex and its interpretation is difficult, as this behavior has not been observed elsewhere. Processes in the soil and karst as well as in-cave processes have to be taken into consideration. High-resolution LA-AMS ^{14}C measurements in conjunction with O isotope data and growth rate changes, however, greatly assist in disentangling the driving mechanism(s) for these $\delta^{13}C$ variations. The dcf between 8.0 aand 3.8 ka BP is generally lower than in the older section. This means that either the aged OM in the karst was depleted or its degradation was reduced, possibly due to a reduction in meteoric precipitation (as deduced from growth rate reduction). Both reasons, less meteoric precipitation and a depleted deep OM pool, would well explain the observed reduction in growth rate. The only speleothem C sources available in this period were consequently the close-to-modern SOM and the radiocarbon-free host rock.

The dcf record shows a strong and rapid increase around 6 ka and a rapid decrease back to pre-6 ka levels at around 5 ka (Fig. 3). The increase in dcf occurs at the same time as a significant decrease in $\delta^{18}O$, but dcf remains elevated when $\delta^{18}O$ jumps back again shortly after. Instead, the decrease in dcf at 5 ka occurs contemporaneously with a $\delta^{13}C$ decrease after $\delta^{13}C$ values remained at elevated values for nearly a millennium. The reason for such a behavior of the dcf remains elusive. In this section, we focus on the cause of the large and rapid jumps in $\delta^{13}C$ by testing two hypotheses.

Hypothesis 1: Processes above the cave, i.e. different carbonate dissolution processes, cause the rapid switching

Two different processes may have caused carbonate dissolution at Spannagel cave in this period. The first involves soil CO_2-derived carbonic acid while the second process operates via sulfuric acid formed by pyrite oxidation (compare Fig. 4 A and B). During times when the first process dominates, the stable carbon isotopic composition of stalagmites is strongly influenced by C from the soil shifting $\delta^{13}C$ towards more negative values. At the same time, the dcf is expected to be relatively low (at least <50%) as the comparably ^{14}C-rich soil C contributes significantly to the signal. In contrast, pyrite oxidation leads to more positive $\delta^{13}C$ values in the stalagmite corresponding to the $\delta^{13}C$ composition of the host rock, as the $\delta^{13}C$-depleted biogenic source contributes little or even no C (Bajo et al., 2017; Spötl et al., 2016). Under these conditions, the dcf should increase to values close to 100% if the comparably modern soil contribution is absent. If the observed $\delta^{13}C$ variations are caused by rapid alternation between both processes, a positive correlation between $\delta^{13}C$ and the dcf has to be expected, with extreme values in the dcf as outlined above. However, no significant long-term positive correlation for the two data series, i.e. $\delta^{13}C$ and dcf, is observed (Fig. S10) and extreme DCF values are not observed. A robust comparison of both data sets is impeded because of the different spatial offset of the two measurement tracks from the growth axis. The radiocarbon track is located ca. 5 mm further from the central growth axis than the stable isotope track (Fig. 2). Growth layers cannot be identified, but the small stalagmite diameter suggests steeply dipping layers resulting in an apparent shift of the dcf towards older ages relative to $\delta^{13}C$. Indeed, such a delay is observable when comparing details in the two data series (Fig. 3 b). Taking a potential offset between the two records into account (see Materials & Methods), a positive correlation between main features in $\delta^{13}C$ and dcf are observable for the middle period, especially between 8 and 6 ka and also partly between 5 and 3.8 ka BP. Those phases are interrupted by the interval of the previously described strong increase in dcf.

9

276   The large swings in $\delta^{13}C$ suggest frequent switches between the carbonate dissolution mechanism from carbonic

277   acid dissolution to pyrite oxidation. However, this is expected to be accompanied by an increase of the dcf to 100%

278   because of the diminishing ^{14}C-rich soil signature, which, however, is not observed. Generally, the dcf is even

279   smaller than in the youngest and oldest sections of the stalagmite, i.e. after 3.8 ka and before 8 ka BP. The

280   correlation between dcf and $\delta^{13}C$ suggests that there might have been a change between open and closed carbonate

281   dissolution regimes, but the magnitude of $\delta^{13}C$ variations found in SPA 127 is larger than if triggered by this

282   process even when changing from a completely open to a completely closed system (Hendy, 1971; Fohlmeister et

283   al., 2011). Thus, additional processes in the cave most likely caused this unusual behavior and the high-magnitude

284   and high-frequency $\delta^{13}C$ variations.

285

10

CARBONATE DISSOLUTION MECHANISM ALTERNATING BETWEEN SOIL CO₂ AND SULFIDE OXIDATION
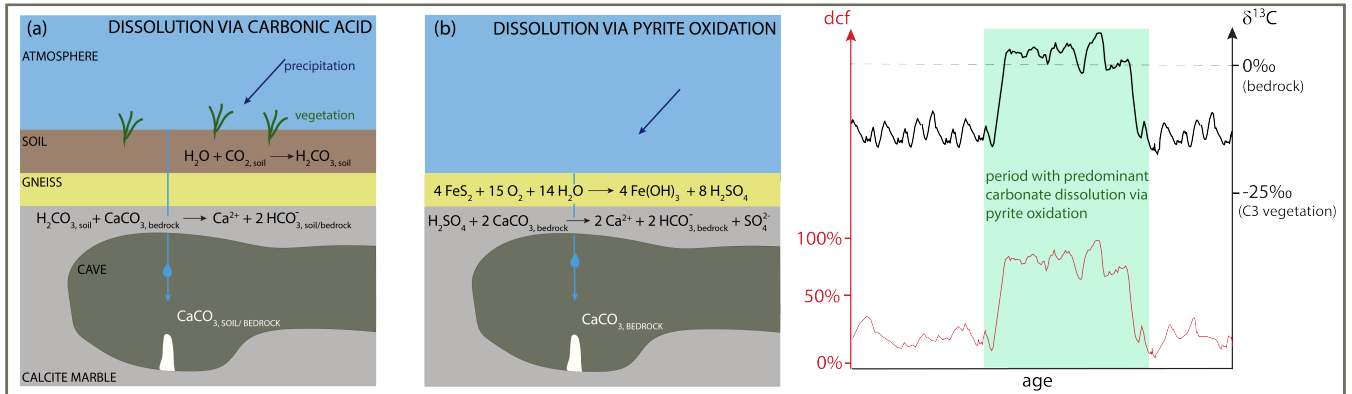
CARBONATE DISSOLUTION MECHANISM: OPEN vs. CLOSED
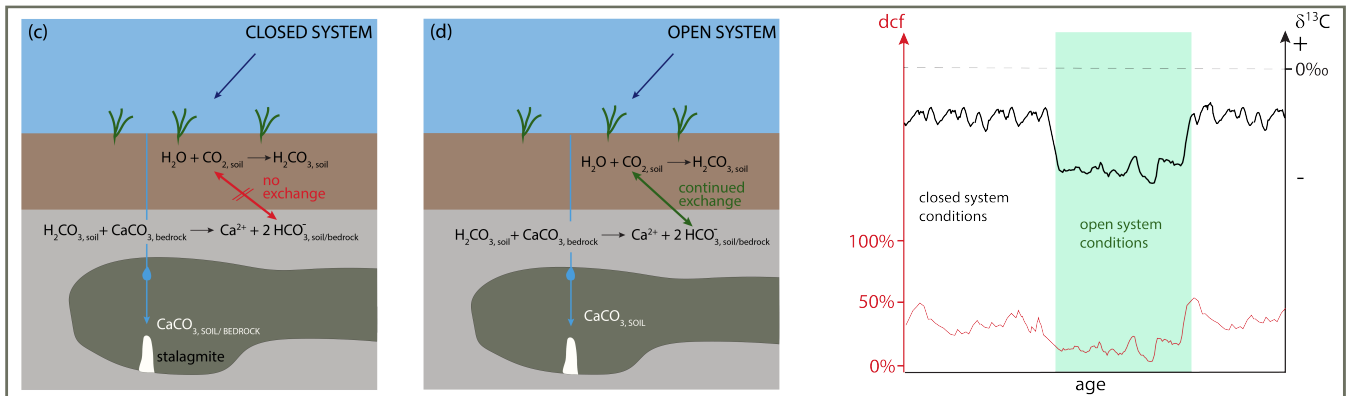
PROCESSES IN CAVE: FRACTIONATION
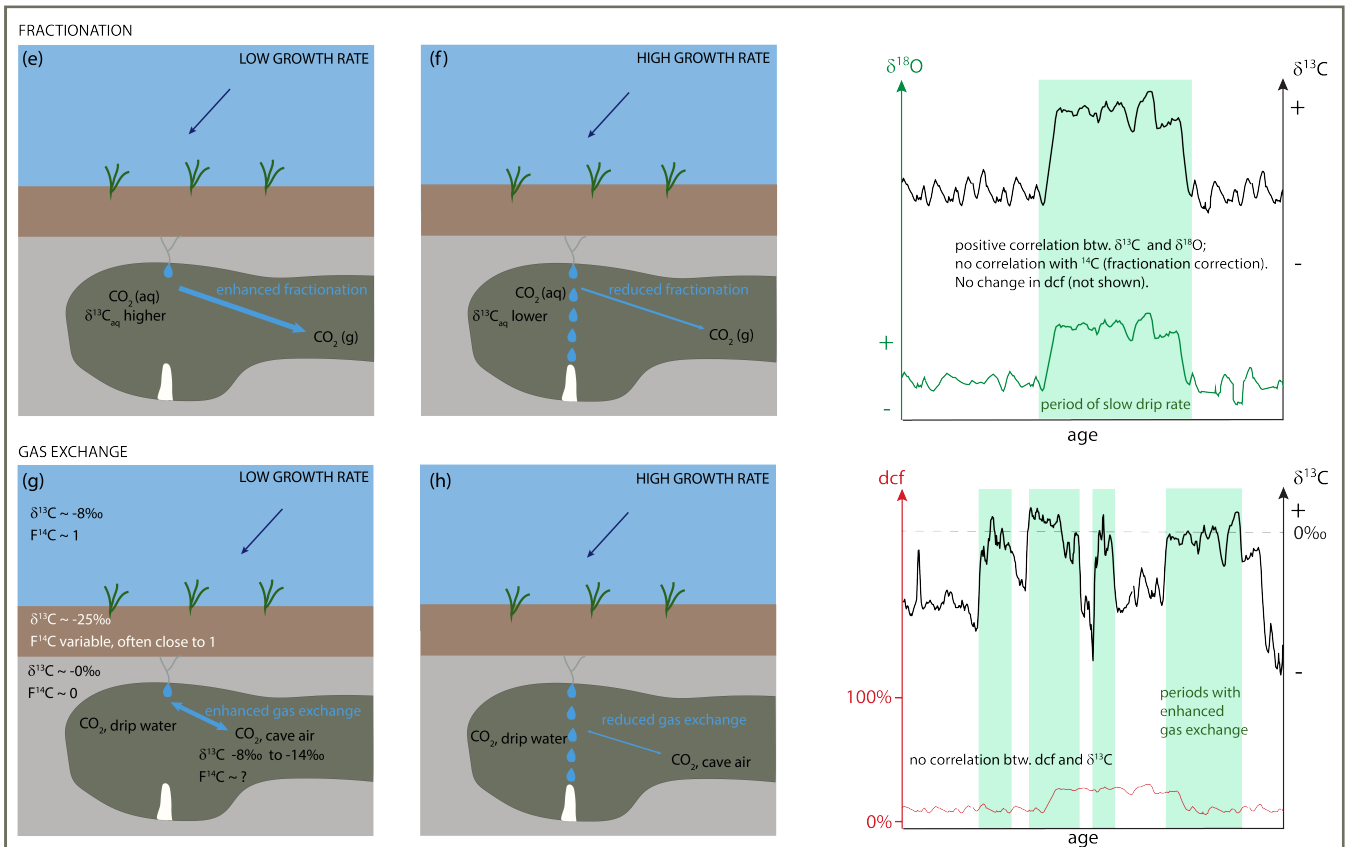
286

287   *Fig. 4 Overview of different processes that can influence $F^{14}C$ and $\delta^{13}C$ in speleothems. For details see text.*

288   • **Hypothesis 2:** Processes in the cave cause the rapid switching

11

289   A major factor influencing the carbon isotope composition of stalagmites are fractionation processes (compare
290   Fig. 4 E and F), which occur during degassing of CO_2 and precipitation of $CaCO_3$ from the solution. Fast dripping
291   results in fast growth and leaves less time for fractionation or C isotope exchange (compare Fig. 4 G and H) and
292   vice versa (e.g., Fohlmeister et al., 2018; Scholz et al., 2009). In addition, the difference in pCO_2 between water
293   and cave-air CO_2 can also influence isotope fractionation and C exchange processes. In the middle part of SPA
294   127, the average growth rate decreased to ≤ 30 μm/a, which is significantly lower than in the oldest section. As
295   discussed earlier, the reduction in growth rate might have been partly induced by reduced meteoric precipitation
296   resulting in slower drip rates or by reduced soil or karst CO_2 concentrations leading to less dissolved host rock
297   $CaCO_3$. In addition, a lower or absent contribution of an "old" OM reservoir in the karst would have led to a lower
298   pCO_2 difference between the CO_2 concentration in the drip water and cave air, which favors an increase in $\delta^{13}C$
299   through fractionation and C isotope exchange processes in the cave. We hypothesize that the rapid changes in $\delta^{13}C$
300   might correlate with short-term changes in growth rate, which cannot be resolved by the available U-Th
301   chronology, enabling or disabling isotope fractionation and gas exchange in the cave that are described in the
302   following two paragraphs.

303   (i)   Changes in fractionation effects

304   During periods of slow growth, fractionation processes can significantly alter the isotopic composition of the
305   stalagmite. During CO_2 degassing from the drip water, the lighter molecules are preferentially transferred
306   into the gas phase resulting in a solution enriched in heavy isotopes. Indeed, recent experiments (Fahrni et
307   al., 2017) support earlier findings that fractionation of radiocarbon relative to ^{12}C is about twice as large as
308   for ^{13}C relative to ^{12}C (Stuiver and Robinson, 1974). However, as radiocarbon measurements are corrected
309   for fractionation effects via $\delta^{13}C$ values, it is impossible to detect a potential correlation between the two
310   isotopes due to fractionation effects. However, potential fractionation affecting $\delta^{13}C$ also influences $\delta^{18}O$ and
311   can be confirmed by a positive correlation between stable C isotopes and O isotopes, e.g. (Dreybrodt, 2008;
312   Polag et al., 2010). Applying a running correlation coefficient between $\delta^{13}C$ and $\delta^{18}O$ is a powerful tool to
313   detect fractionation changes through time (Fohlmeister et al., 2017). 11-point running correlation coefficients
314   calculated for the two time series of SPA 127 show no stalagmite sections with a high correlation coefficient,
315   but vary without any obvious pattern between -1 and +1 (compare Fig. S10, bottom panel). Thus,
316   fractionation was most likely not the main process causing the large variations in $\delta^{13}C$, but may have played
317   a minor role during some periods.

318   (ii)   Prior calcite precipitation (PCP)

319   PCP can have an effect on $\delta^{13}C$, even a large ones as observed for our stalagmite. While this would not have
320   an effect on ^{14}C, we would expect that $\delta^{18}O$ should show a similar behavior, which is not the case. Thus, we
321   can safely assume, that PCP is not responsible for the rapid changes observed in SPA 127.

322   (iii)   Gas exchange processes

323   Another process that is a potential candidate for causing the behavior observed in SPA 127 in this interval is
324   the C isotope exchange between CO_2 of the cave air and C dissolved in the drip water. The gas exchange
325   process may be dominant if the stalagmite growth rate is sufficiently low and when drip intervals are long
326   and/or the differences between the pCO_2 of the water and cave air is small (Hendy, 1971; Scholz et al., 2009).

12

In this case, the C isotopic composition of the drip water when reaching the top of the stalagmite depends mainly on the initial $\delta^{13}C$ of drip water and on the degree of C isotope exchange with the cave atmosphere. Spannagel Cave is well ventilated throughout the year with cave air $\delta^{13}C$ values of -10 to -11‰ (Töchterle et al., 2017), which is significantly lower than that of the atmosphere, i.e. approximately -8‰ (Keeling et al., 2010). These more negative values are a hint towards a contribution from soil air. The following assumptions were made: the $\delta^{13}C$ of drip water is composed of two biogenic C sources ($\delta^{13}C \sim$ -25‰) and host rock ($\delta^{13}C \sim$ 0‰) and about 20 - 30% are derived from the host rock (based on the dcf in this interval). Accounting for about 10‰ to 11‰ fractionation between soil gas CO_2 and HCO_3^- during the transition of soil gas CO_2 to dissolved inorganic carbon (DIC), the initial drip water, which was feeding the stalagmite, had a $\delta^{13}C$ value between -11.5 and -9‰ (Mook et al., 1974). Considering Rayleigh fractionation effects in the cave, carbonate $\delta^{13}C$ values of -8‰ appear feasible (Scholz et al., 2009, Deininger et al., 2012) without any exchange of C isotopes. C isotope exchange processes lead to water significantly enriched in ^{13}C. When cave air with $\delta^{13}C$ values around -11‰ exchanges with drip water, the C isotopic composition of the water will increase, as the transition of gaseous CO_2 to HCO_3^- involves a fractionation of about +10 to +11‰ at temperatures between 0 and 5°C. Thus, drip water in C isotopic equilibrium with cave air CO_2, which is the most extreme case, should have $\delta^{13}C$ values of -1 to 0‰. Precipitation of $CaCO_3$ from such water would result in $\delta^{13}C$ values of around 0 to +1‰ as observed for some short intervals.

Similar considerations can be applied to radiocarbon. If the cave ventilation is sluggish, $F^{14}C$ in the cave air will deviate from atmospheric values (i.e. $F^{14}C_{atm} \approx 1$) as it is influenced by other sources, such as soil air or CO_2 degassed from drip water, which both are depleted with respect to atmospheric values. In a recent study, cave air has been shown to be depleted in radiocarbon with values as low as $F^{14}C \approx 0.6$ (Minami et al., 2015). When the cave ventilation is not effectively changing the depleted radiocarbon towards more atmospheric values, C isotope exchange processes are not detectable using ^{14}C in speleothems. As isotopic fractionation is not important for radiocarbon (as explained above), C isotope exchange of DIC with cave air, which both have a similar radiocarbon content, would have no effect on the ^{14}C signal of the precipitated calcite.

In summary, combined high-resolution $\delta^{13}C$ and radiocarbon measurements are a valuable tool to shed new light on processes affecting C isotopes in the subsurface. Using well justified assumptions and first-order calculations of mixing and fractionation effects, in-cave C isotope exchange processes remain the only explanation for the rapid and high-magnitude $\delta^{13}C$ changes.

5.3 Interpretation of dcf and δ13C in the youngest section of SPA 127 (3.8 to 2.5 ka BP)

In the youngest section of this stalagmite a behavior similar to the oldest section with respect to $\delta^{13}C$ and radiocarbon content is observed. From approximately 3.8 ka BP onward, the dcf increases slowly from about 20% to 50%. Correspondingly, $\delta^{13}C$ shows a lower variability than in the middle part with mean $\delta^{13}C$ values of -3‰ to -4‰, which is also comparable to the behavior observed for the interval > 8 ka BP. As $\delta^{13}C$ does not show any long-term trend as observed for the reservoir effect, we rule out a change to more closed carbonate dissolution conditions driving the increase in dcf. The only explanation that can lead to such an increase is an "old" C reservoir. We propose that climatic conditions changed such that this "old" OM pool in the karst, which was decoupled from the atmosphere, has become the main OM derived CO_2 source. This CO_2 resulted in acidification in a comparable way as soil CO_2 enhancing carbonate dissolution and ultimately contributed to stalagmite $CaCO_3$. The isotopic ^{14}C imprint, however, is significantly different to soil CO_2 causing the observed increase in dcf. Between

13

approximately 8 and 6 ka BP the Alps experienced a warmer climate than today (Ivy-Ochs et al., 2009; Nicolussi et al., 2005). A study conducted by Nicolussi et al. (2005) in the Kauner valley, situated approximately 70 km west of Spannagel Cave, showed that the timberline was significantly higher during that period (Fig. 5) supporting a warmer climate. Between 6 and 4 ka BP the timberline was comparable to the present-day situation.
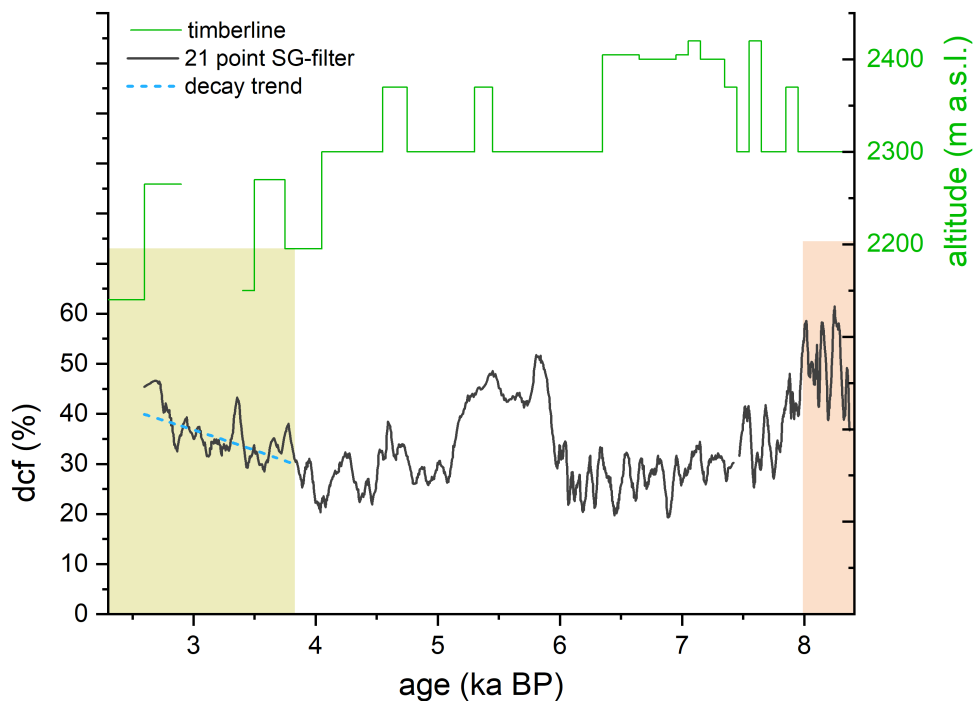
Figure 5: Comparison of the dcf in stalagmite SPA 127 with the elevation of the timberline reconstructed for the Kauner valley 70 km west of Spannagel Cave (green line, after Nicolussi et al. (2005)) with the dcf. Around 4 ka BP the timberline started to decline which is concurrent with an increase in dcf, i.e., a decrease in initial ^{14}C. This decrease closely follows a radiocarbon decay trend (dashed blue line). Green and red areas mark the three different time periods as indicated in Fig. 4.

It is expected that with the lowering of the timberline after ~4 ka the vegetation density decreased as well, which should be reflected in the speleothem- $\delta^{13}C$ values. This, however, is not the case during this period pointing towards a relatively stable contribution of soil-derived CO_2. Possibly, a certain proportion of plants that grew during the early to mid-Holocene warm epoch died and the corresponding OM located in the deeper vadose zone was initially stabilized due to reduced meteoric precipitation and later became mobilized due to enhanced microbial activity. Considering the low mean annual temperatures at this high-alpine site, decomposition processes are most likely slow, allowing OM to age during decomposition as indicated in a recent study by Shi et al. (2020). The radiocarbon composition of the ageing SOM will closely follow a radiocarbon-specific exponential decay and is responsible for the depleted radiocarbon concentration in soil gas CO_2. Depending on the contribution of root-respired CO_2 of Alpine plants compared to the decomposed CO_2 from dead OM, the dcf will closely follow an exponential decay, resembling that of the radiocarbon decay and thus would contribute to the observed increase of the dcf. The closer the observed increase in the dcf follows that of a radiocarbon decay trajectory, the larger the contribution of CO_2 from the aging SOM reservoir in relation to root-respired CO_2. Based on the observed rate of increase in dcf, which compares well with the radiocarbon decay trend (blue dashed line in Fig. 5), we suggest that the majority of DIC that contributed to the speleothem $CaCO_3$ had its origin in aged soil OM.

14

6 Conclusion

Combined stable carbon isotope and radiocarbon analyses of stalagmite SPA 127 provide a comprehensive picture of the carbon dynamics at the Spannagel Cave. Due to the novel LA-AMS technique, a highly spatially resolved ^{14}C time series allows unprecedented insights into processes in this high-alpine karst system. Care has to be taken when applying LA-AMS to stalagmites as epoxy resin used in sample preparation leads to distorted results.

Results from this study allow to distinguish three intervals with different carbon dynamics:

(i) The interval before 8 ka BP is characterized by generally low and stable $\delta^{13}C$ values combined with a comparably high dcf (>50%) pointing towards the existence of an "old" OM reservoir in the epikarst. CO_2 emanating from this presaged C pool provides additional carbonic acid potentially enhancing bedrock dissolution.

(ii) The interval between 8 and 3.8 ka BP is characterized by a strong variability in $\delta^{13}C$ with a generally lower dcf suggesting that the "old" OM reservoir in the karst had either been exhausted or stabilized (less production to aged respired soil/karst CO_2) possibly due to reduced meteoric precipitation. This is supported by a lower stalagmite growth rate in this period. In-cave gas exchange processes are the most likely explanation for the strong $\delta^{13}C$ variability, as (i) bedrock dissolution mechanisms, i.e. pyrite oxidation vs. carbonic acid dissolution, are not supported by the magnitude of changes in dcf and stable C, even though the temporal coherence indicates that some of the $\delta^{13}C$ variations might be explained by the bedrock dissolution mode (open vs. closed carbonate dissolution) and, (ii) fractionation processes in the cave cannot explain the large shifts as no correlation between $\delta^{18}O$ and $\delta^{13}C$ is observed.

(iii) In the interval between 3.8 and 2.4 ka BP the comparably more stable $\delta^{13}C$ signature combined with an increasing dcf hints towards a contribution from an ageing OM reservoir in the karst similar to the period > 8 ka BP. This OM reservoir contributed to the stalagmite growth in this period due to warmer climatic conditions. While the contribution of "old" OM in the oldest growth phase was stable, the youngest section indicates an ageing of this reservoir.

Author contribution

CW, JF and CS conceptualized the content of this manuscript. CW, MW, BH carried LA-AMS measurements out, CS conducted stable carbon isotope analyses. MW and LW developed the data reduction strategy. JF, CW and TE interpreted the data and compared them to published records. CW prepared the manuscript with contributions from all co-authors.

Competing interests

The authors declare that they have no conflict of interest.

References

Bajo, P., Borsato, A., Drysdale, R., Hua, Q., Frisia, S., Zanchetta, G., Hellstrom, J., and Woodhead, J.: Stalagmite carbon isotopes and dead carbon proportion (DCP) in a near-closed-system situation: An interplay between sulphuric and carbonic acid dissolution, Geochimica et Cosmochimica Acta, 210, 208-227, 2017.

Bar-Matthews, M., Ayalon, A., Kaufman, A., and Wasserburg, G. J.: The Eastern Mediterranean paleoclimate as a reflection of regional events: Soreq cave, Israel, Earth and Planetary Science Letters, 166, 85-95, 1999.

Benavente, J., Vadillo, I., Carrasco, F., Soler, A., Liñán, C., and Moral, F.: Air carbon dioxide contents in the vadose zone of a Mediterranean karst, Vadose Zone Journal, 9, 126-136, 2010.

Bergel, S. J., Carlson, P. E., Larson, T. E., Wood, C. T., Johnson, K. R., Banner, J. L., and Breecker, D. O.: Constraining the subsoil carbon source to cave-air CO_2 and speleothem calcite in central Texas, Geochimica et Cosmochimica Acta, 217, 112-127, 2017.

Breecker, D. O., Payne, A. E., Quade, J., Banner, J. L., Ball, C. E., Meyer, K. W., and Cowan, B. D.: The sources and sinks of CO_2 in caves under mixed woodland and grassland vegetation, Geochimica et Cosmochimica Acta, 96, 230-246, 2012.

Cheng, H., Edwards, R. L., Sinha, A., Spötl, C., Yi, L., Chen, S., Kelly, M., Kathayat, G., Wang, X., Li, X., Kong, X., Wang, Y., Ning, Y., and Zhang, H.: The Asian monsoon over the past 640,000 years and ice age terminations, Nature, 534, 640-646, 2016.

Denniston, R. F., DuPree, M., Dorale, J. A., Asmerom, Y., Polyak, V. J., and Carpenter, S. J.: Episodes of late Holocene aridity recorded by stalagmites from Devil's Icebox Cave, central Missouri, USA, Quaternary Research, 68, 45-52, 2007.

Dreybrodt, W.: Evolution of the isotopic composition of carbon and oxygen in a calcite precipitating H_2O–CO_2–$CaCO_3$ solution and the related isotopic composition of calcite in stalagmites, Geochimica et Cosmochimica Acta, 72, 4712-4724, 2008.

Fahrni, S. M., Southon, J. R., Santos, G. M., Palstra, S. W., Meijer, H. A., and Xu, X.: Reassessment of the 13C/12C and 14C/12C isotopic fractionation ratio and its impact on high-precision radiocarbon dating, Geochimica et Cosmochimica Acta, 213, 330-345, 2017.

Fairchild, I. J. and Baker, A.: Speleothem science: from process to past environments, John Wiley & Sons, 2012.

Fairchild, I. J., Smith, C. L., Baker, A., Fuller, L., Spötl, C., Mattey, D., and McDermott, F.: Modification and preservation of environmental signals in speleothems, Earth-Science Reviews, 75, 105-153, 2006.

Fohlmeister, J., Arps, J., Spötl, C., Schröder-Ritzrau, A., Plessen, B., Günter, C., Frank, N., and Trüssel, M.: Carbon and oxygen isotope fractionation in the water-calcite-aragonite system, Geochimica et Cosmochimica Acta, 235, 127-139, 2018.

Fohlmeister, J., Kromer, B., and Mangini, A.: The influence of soil organic matter age spectrum on the reconstruction of atmospheric C-14 levels via stalagmites, Radiocarbon, 53, 99-115, 2011a.

Fohlmeister, J., Plessen, B., Dudashvili, A. S., Tjallingii, R., Wolff, C., Gafurov, A., and Cheng, H.: Winter precipitation changes during the Medieval Climate Anomaly and the Little Ice Age in arid Central Asia, Quaternary Science Reviews, 178, 24-36, 2017.

Fohlmeister, J., Scholz, D., Kromer, B., and Mangini, A.: Modelling carbon isotopes of carbonates in cave drip water, Geochimica et Cosmochimica Acta, 75, 5219-5228, 2011b.

Fohlmeister, J., Schröder-Ritzrau, A., Spötl, C., Frisia, S., Miorandi, R., Kromer, B., and Mangini, A.: The Influences of Hydrology on the Radiogenic and Stable Carbon Isotope Composition of Cave Drip Water, Grotta di Ernesto (Italy), Radiocarbon, 52, 1529-1544, 2010a.

Fohlmeister, J., Schroeder-Ritzrau, A., Spoetl, C., Frisia, S., Miorandi, R., Kromer, B., and Mangini, A.: The influences of hydrology on the radiovenic and stable carbon isotope composition of cave drip water, Grotta die Ernesto (Italy), Radiocarbon, 52, 1529-1544, 2010b.

Fohlmeister, J., Voarintsoa, N. R. G., Lechleitner, F. A., Boyd, M., Brandtstätter, S., Jacobson, M. J., and L. Oster, J.: Main controls on the stable carbon isotope composition of speleothems, Geochimica et Cosmochimica Acta, 279, 67-87, 2020.

16

478 Fohlmeister, J., Vollweiler, N., Spötl, C., and Mangini, A.: COMNISPA II: Update of a mid-European
479 isotope climate record, 11 ka to present, The Holocene, 23, 749-754, 2013.
480 Genty, D. and Massault, M.: Bomb 14 C recorded in laminated speleothems: calculation of dead carbon
481 proportion, Radiocarbon, 39, 33-48, 1997.
482 Gray, A. L.: Solid sample introduction by laser ablation for inductively coupled plasma source-mass
483 spectrometry, Analyst, 110, 551-556, 1985.
484 Griffiths, M., Fohlmeister, J., Drysdale, R. N., Hua, Q., Johnson, K., Hellstrom, J. C., Gagan, M., and Zhao,
485 J.-X.: Hydrological control of the dead carbon fraction in a Holocene tropical speleothem, Quat.
486 Geochronol., 14, 81-93, 2012.
487 Hendy, C. H.: The isotopic geochemistry of speleothems—I. The calculation of the effects of different
488 modes of formation on the isotopic composition of speleothems and their applicability as
489 palaeoclimatic indicators, Geochimica et cosmochimica Acta, 35, 801-824, 1971.
490 Ivy-Ochs, S., Kerschner, H., Maisch, M., Christl, M., Kubik, P. W., and Schlüchter, C.: Latest Pleistocene
491 and Holocene glacier variations in the European Alps, Quaternary Science Reviews, 28, 2137-2149,
492 2009.
493 Keeling, R., Piper, S., Bollenbacher, A., and Walker, S.: Monthly atmospheric 13C/12C isotopic ratios
494 for 11 SIO stations, Trends: a compendium of data on global change, 2010. 2010.
495 Koch, J. and Guenther, D.: Review of the State-of-the-Art of Laser Ablation Inductively Coupled Plasma
496 Mass Spectrometry, Applied Spectroscopy, 65, 155A-162A, 2011.
497 Kutschera, W.: Applications of accelerator mass spectrometry, International Journal of Mass
498 Spectrometry, 349, 203-218, 2013.
499 Lachniet, M. S.: Climatic and environmental controls on speleothem oxygen-isotope values,
500 Quaternary Science Reviews, 28, 412-432, 2009.
501 Lauritzen, S.-E.: Marble stripe karst of the Scandinavian Caledonides: an end-member in the contact
502 karst spectrum, Slovenska akademija znanosti in umetnosti, 2001.
503 Lechleitner, F. A., Baldini, J. U., Breitenbach, S. F., Fohlmeister, J., McIntyre, C., Goswami, B., Jamieson,
504 R. A., van der Voort, T. S., Prufer, K., and Marwan, N.: Hydrological and climatological controls on
505 radiocarbon concentrations in a tropical stalagmite, Geochimica et Cosmochimica Acta, 194, 233-252,
506 2016.
507 Mangini, A., Spötl, C., and Verdes, P.: Reconstruction of temperature in the Central Alps during the
508 past 2000 yr from a δ18O stalagmite record, Earth and Planetary Science Letters, 235, 741-751, 2005.
509 Mattey, D. P., Atkinson, T. C., Barker, J. A., Fisher, R., Latin, J. P., Durrell, R., and Ainsworth, M.: Carbon
510 dioxide, ground air and carbon cycling in Gibraltar karst, Geochimica et Cosmochimica Acta, 184, 88-
511 113, 2016.
512 Minami, M., Kato, T., Horikawa, K., and Nakamura, T.: Seasonal variations of 14C and δ13C for cave
513 drip waters in Ryugashi Cave, Shizuoka Prefecture, central Japan, Nuclear Instruments and Methods in
514 Physics Research Section B: Beam Interactions with Materials and Atoms, 362, 202-209, 2015.
515 Mook, W., Bommerson, J., and Staverman, W.: Carbon isotope fractionation between dissolved
516 bicarbonate and gaseous carbon dioxide, Earth and Planetary science letters, 22, 169-176, 1974.
517 Moseley, G. E., Spötl, C., Brandstätter, S., Erhardt, T., Luetscher, M., and Edwards, R. L.: NALPS19: sub-
518 orbital-scale climate variability recorded in northern Alpine speleothems during the last glacial period,
519 Climate of the Past, 16, 29-50, 2020.
520 Nicolussi, K., Kaufmann, M., Patzelt, G., Plicht van der, J., and Thurner, A.: Holocene tree-line variability
521 in the Kauner Valley, Central Eastern Alps, indicated by dendrochronological analysis of living trees and
522 subfossil logs, Vegetation History and Archaeobotany, 14, 221-234, 2005.
523 Noronha, A. L., Johnson, K. R., Hu, C., Ruan, J., Southon, J. R., and Ferguson, J. E.: Assessing influences
524 on speleothem dead carbon variability over the Holocene: Implications for speleothem-based
525 radiocarbon calibration, Earth and Planetary Science Letters, 394, 20-29, 2014.
526 Noronha, A. L., Johnson, K. R., Southon, J. R., Hu, C. Y., Ruan, J. Y., and McCabe-Glynn, S.: Radiocarbon
527 evidence for decomposition of aged organic matter in the vadose zone as the main source of
528 speleothem carbon, Quaternary Science Reviews, 127, 37-47, 2015.

17

529 Polag, D., Scholz, D., Mühlinghaus, C., Spötl, C., Schröder-Ritzrau, A., Segl, M., and Mangini, A.: Stable
530 isotope fractionation in speleothems: Laboratory experiments, Chemical Geology, 279, 31-39, 2010.
531 Reimer, P. J., Bard, E., Bayliss, A., Beck, J. W., Blackwell, P. G., Ramsey, C. B., Buck, C. E., Cheng, H.,
532 Edwards, R. L., Friedrich, M., Grootes, P. M., Guilderson, T. P., Haflidason, H., Hajdas, I., Hatté, C.,
533 Heaton, T. J., Hoffmann, D. L., Hogg, A. G., Hughen, K. A., Kaiser, K. F., Kromer, B., Manning, S. W., Niu,
534 M., Reimer, R. W., Richards, D. A., Scott, E. M., Southon, J. R., Staff, R. A., Turney, C. S. M., and van der
535 Plicht, J.: IntCal13 and Marine13 Radiocarbon Age Calibration Curves 0–50,000 Years cal BP,
536 Radiocarbon, 55, 1869-1887, 2013.
537 Richards, D. A. and Dorale, J. A.: Uranium-series chronology and environmental applications of
538 speleothems, Rev. Mineral, 52, 407-460, 2003.
539 Savitzky, A. and Golay, M. J. E.: Smoothing and Differentiation of Data by Simplified Least Squares
540 Procedures, Analytical Chemistry, 36, 1627-1639, 1964.
541 Scholz, D. and Hoffmann, D.: ^{230}Th/U-dating of fossil reef corals and speleothems, Quater. Sci. J., 57,
542 52-77, 2008.
543 Scholz, D. and Hoffmann, D. L.: StalAge - An algorithm designed for construction of speleothem age
544 models, Quat. Geochronol., 6, 369-382, 2011.
545 Scholz, D., Mühlinghaus, C., and Mangini, A.: Modelling δ13C and δ18O in the solution layer on
546 stalagmite surfaces, Geochimica et Cosmochimica Acta, 73, 2592-2602, 2009.
547 Shi, Z., Allison, S. D., He, Y., Levine, P. A., Hoyt, A. M., Beem-Miller, J., Zhu, Q., Wieder, W. R., Trumbore,
548 S., and Randerson, J. T.: The age distribution of global soil carbon inferred from radiocarbon
549 measurements, Nat. Geosci., 13, 555-559, 2020.
550 Southon, J., Noronha, A. L., Cheng, H., Edwards, R. L., and Wang, Y.: A high-resolution record of
551 atmospheric 14C based on Hulu Cave speleothem H82, Quaternary Science Reviews, 33, 32-41, 2012.
552 Spötl, C.: Long-term performance of the Gasbench isotope ratio mass spectrometry system for the
553 stable isotope analysis of carbonate microsamples, Rapid Communications in Mass Spectrometry, 25,
554 1683-1685, 2011.
555 Spötl, C., Fairchild, I. J., and Tooth, A. F.: Cave air control on dripwater geochemistry, Obir Caves
556 (Austria): Implications for speleothem deposition in dynamically ventilated caves, Geochimica et
557 Cosmochimica Acta, 69, 2451-2468, 2005.
558 Spötl, C., Fohlmeister, J., Cheng, H., and Boch, R.: Modern aragonite formation at near-freezing
559 conditions in an alpine cave, Carnic Alps, Austria, Chemical geology, 435, 60-70, 2016.
560 Spötl, C. and Mangini, A.: Paleohydrology of a high-elecation, glacier influenced karst system in the
561 central alps (Austria), Austrian Journal of Earth Sciences, 103, 92-105, 2010.
562 Spötl, C. and Mangini, A.: Speleothems and paleoglaciers, Earth and Planetary Science Letters, 254,
563 323-331, 2007.
564 Spötl, C., Mangini, A., Bums, S. J., Frank, N., and Pavuza, R.: Speleothems from the high-alpine
565 Spannagel cave, Zillertal Alps (Austria). In: Studies of cave sediments, Springer, 2004.
566 Spötl, C. and Mattey, D.: Stable isotope microsampling of speleothems for palaeoenvironmental
567 studies: A comparison of microdrill, micromill and laser ablation techniques, Chem.Geol., 235, 48-58,
568 2006.
569 Stuiver, M. and Robinson, S. W.: University of Washington GEOSECS north Atlantic carbon-14 results,
570 Earth and Planetary Science Letters, 23, 87-90, 1974.
571 Therre, S., Fohlmeister, J., Fleitmann, D., Matter, A., Burns, S. J., Arps, J., Schröder-Ritzrau, A., Friedrich,
572 R., and Frank, N.: Climate-induced speleothem radiocarbon variability on Socotra Island from the Last
573 Glacial Maximum to the Younger Dryas, Climate of the Past, 16, 409-421, 2020.
574 Töchterle, P., Dublyansky, Y., Stöbener, N., Mandić, M., and Spötl, C.: High-resolution isotopic
575 monitoring of cave air CO2, Rapid Communications in Mass Spectrometry, 31, 895-900, 2017.
576 Wackerbarth, A., Scholz, D., Fohlmeister, J., and Mangini, A.: Modelling the δ18O value of cave drip
577 water and speleothem calcite, Earth and Planetary Science Letters, 299, 387-397, 2010.
578 Welte, C., Wacker, L., Hattendorf, B., Christl, M., Fohlmeister, J., Breitenbach, S. F., Robinson, L. F.,
579 Andrews, A. H., Freiwald, A., and Farmer, J. R.: Laser Ablation–Accelerator Mass Spectrometry: An

580 Approach for Rapid Radiocarbon Analyses of Carbonate Archives at High Spatial Resolution, Analytical
581 chemistry, 88, 8570-8576, 2016a.
582 Welte, C., Wacker, L., Hattendorf, B., Christl, M., Koch, J., Synal, H.-A., and Günther, D.: Novel Laser
583 Ablation Sampling Device for the Rapid Radiocarbon Analysis of Carbonate Samples by Accelerator
584 Mass Spectrometry, Radiocarbon, 58, 419-435, 2016b.
585 Welte, C., Wacker, L., Hattendorf, B., Christl, M., Koch, J., Yeman, C., Breitenbach, S. F. M., Synal, H. A.,
586 and Gunther, D.: Optimizing the analyte introduction for C-14 laser ablation-AMS, Journal of Analytical
587 Atomic Spectrometry, 32, 1813-1819, 2017.
588 Yeman, C., Christl, M., Hattendorf, B., Wacker, L., Welte, C., Brehm, N., and Synal, H. A.: Unravelling
589 Quasi-Continuous 14C Profiles by Laser Ablation AMS, Radiocarbon, 62, 453-465, 2020.

590

591